

Study of inter-individual variability of three-dimensional data table: detection of unstable variables and samples

Loïc Labache^{1, 2}, Marc Joliot¹, Gaelle E. Doucet³, Jérôme Saracco²

Running title:

SIMS: Similarity of Individual Matrices

¹ Groupe d’Imagerie Neurofonctionnelle – CEA & Institut des Maladies Neurodégénératives de Bordeaux, UMR 5293 - Centre Broca Nouvelle-Aquitaine, 146 rue Léo Saignat, 33000 Bordeaux, France

² Inria Bordeaux Sud Ouest & Institut de Mathématiques de Bordeaux, UMR CNRS 5251 & ENSC Bordeaux INP, 109 Avenue Roul, 33400 Talence, France

³ Boys Town National Research Hospital, Omaha, NE, USA

Abstract

We propose two methodologies to better understand the inter-individual variability of functional Magnetic Resonance Imaging (MRI) brain data. The aim is to quantify whether the “average” dendrogram is representative of the initial population and to identify its possible sources of instability. The first method identifies networks that can lead to unstable partitions of the “average” dendrogram. The second approach identifies homogeneous subpopulations of subjects for whom their associated “average” dendrograms are more stable than that of the original population. These two methods are illustrated on simulated data from intrinsic connectivity data obtained by functional MRI (Magnetic Resonance Imaging). The two suggested approaches to detect an unstable network or the presence of subpopulations have shown good numerical behavior when the noise level does not mask the structure of the data. A real case study is also provided.

Keywords: Hierarchical clustering · Inter-individual variability · Detection of sources of instability

1. Introduction

The analysis of the partitions stability of a dendrogram is a crucial issue in order to check the replicability of the selected partitions.

For classical two-dimensional data, it is possible to obtain a measure of the stability of the clusters (obtained from a given partition) using the approximately unbiased p-value (AU-value) obtained with a multiscale bootstrap resampling method (MBR: Efron 1985) available via the "pvclust" function of the R library of the same name (Suzuki et al. 2006). The AU-value then indicates the unbiased frequency of occurrence of a cluster across the reference population of the dendrogram.

There is currently no counterpart to this method for three-dimensional data. This paper thus develops a similar method to pvclust adapted to any kind of three-dimensional data and in particular for resting-state functional Magnetic Resonance Imaging (rs-fMRI) data.

fMRI allows to obtain regional brain electrical activity (Logothetis et al. 2001, Schummers et al. 2008) by monitoring relative fluctuations in blood oxygenation: this is the BOLD (Blood Oxygen Level Dependent) signal.

The study of humans' brain resting state functional organization consists in studying the synchronicity between the BOLD signals of different brain areas or networks. Commonly, the synchronicity study is performed using the calculation of Pearson correlation coefficients between the BOLD signals of all network pairs, resulting in correlation matrices of dimension $K*K$ for K brain networks. There are databases (of several hundred individuals) containing 3D structures (of dimension $S*K*K$) that gather all the correlation matrices M_s , $s = 1, \dots, S$ of the S individuals in the database.

For a given database (here, the BIL&GIN database, Mazoyer et al., 2016), the first work consisted in an agglomerative hierarchical clustering of K brain networks. The second step was to find an optimal number of clusters reflecting at best the resting state cerebral organisation (Doucet et al., 2011). The methodology consisted in averaging all the Fisher transformations of the matrices M_s in the following way:

$$M_m = \tanh\left(\sum_{s=1}^S \operatorname{arctanh}(M_s)/S\right).$$

This matrix is then transformed into a dissimilarity matrix D_m : $D_m = (1 - M_m)/2$. Then, the aggregation of the K brain networks is accomplished by the agglomerative hierarchical clustering (according to Ward's method) based on D_m .

In order to take into account the inter-individual variability, Doucet et al. (2011) adapted a procedure called pvclust (Suzuki and Shimodaira, 2004) that allows to assess the uncertainty associated to the different partitions of the hierarchical clustering through a p-value obtained by bootstrapping. The previous methodology provides a Bootstrap Probability p-value (called *BP-value*) and, after correction, an Approximately Unbiased p-value (denoted *AU-value*). The *AU-values* are calculated using the bootstrap values recommended in Suzuki et

al. (2006): either by using 50% to 140% of the sample. These p-values indicate how well the different partitions are supported by the data.

To illustrate this methodology, let us consider a population of 439 subjects. The optimal number of clusters was determined using the R library “*NbClust*” (Charrad et al. 2014). This package provides 30 statistical indices for determining the optimal number of clusters and offers the best clustering scheme from the different results obtained by varying all combinations of the number of clusters for the chosen method, in this case, hierarchical clustering with Ward’s criterion. We selected the number of clusters that satisfied a maximum of indices and found it to be equal to 3. For the corresponding three optimal clusters the associated *BP* and *AU-values* are equal to 100% (Figure 1). Since Suzuki et al. (2006) recommend using *AU-values*, these 3 clusters retained are then perfectly represented by our data. However, the *AU-values* represent the stability of the M_m based clusters and not the empirical frequency of appearance of these clusters across the S subjects, called individual frequencies below. Figure 1 illustrates this aspect. We can see the evolution of the *BP-values* as a function of the proportion of subjects used in the bootstrap sampling, as well as the actual value of the individual frequencies of cluster occurrence. For example, for the considered partition into 3 clusters, the corresponding three *BP-values* are 100% whereas the individual frequencies of appearance are respectively 5%, 4% and 12% for these 3 clusters. The individual frequencies of occurrence correspond to the number of times a cluster appears among the individual dendrograms of the population. In the study of intrinsic brain organization, these proportions are unreliable and in a general framework, this shows that the *pvclust* algorithm cannot be used for three-dimensional data: the BP-values do not reflect the individual frequencies.

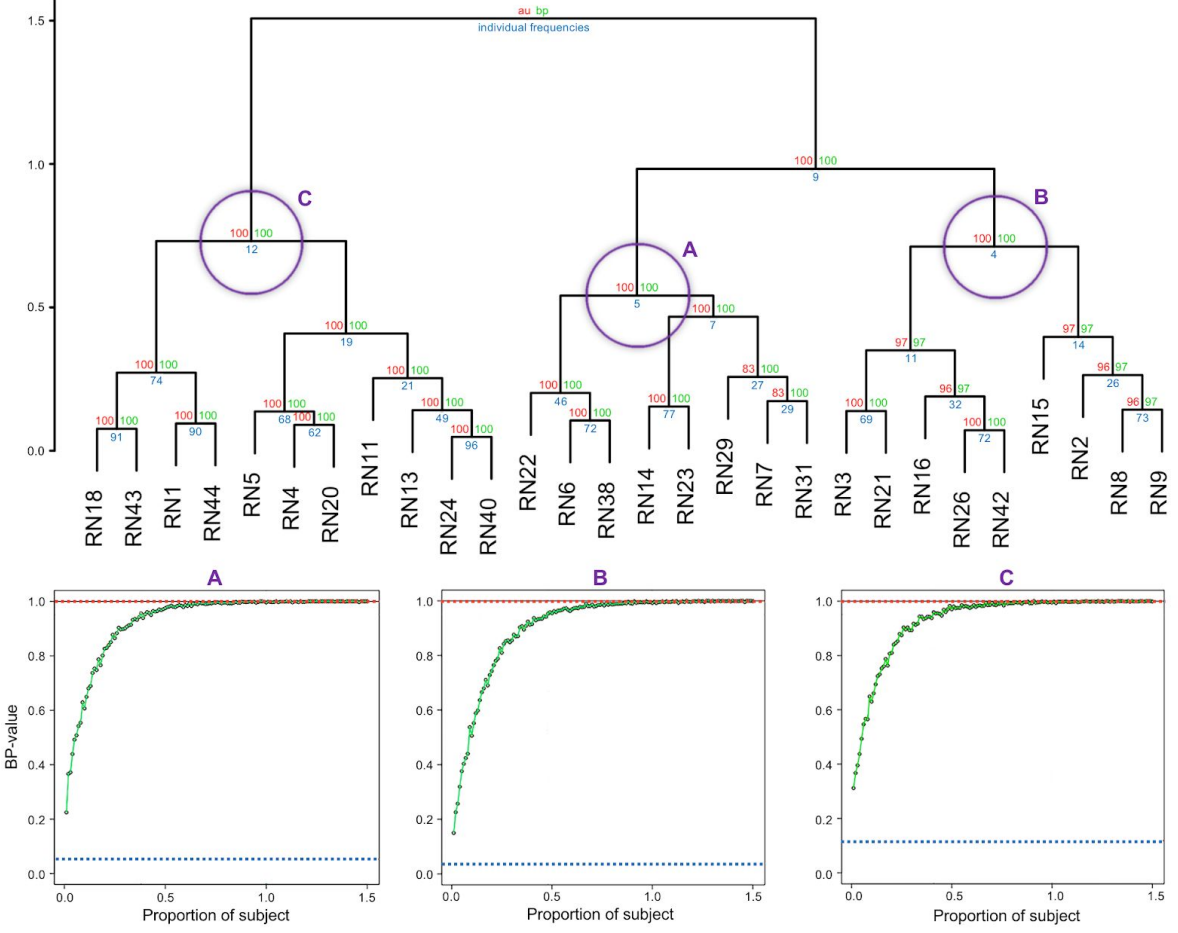


Figure 1: Agglomerative hierarchical clustering from M_m (top). Evolution of *BP-value* as a function of the proportion of individuals sampled in the bootstrap (below). In blue, the individual frequency of the clusters . In green, the *BP-values*. In red, the *AU-values*.

In this paper, two methodologies are proposed to better understand the inter-individual variability of partitions from M_m :

- the first one allows to identify networks that can lead to unstable partitions from M_m ;
- the second one allows to identify, across the population, homogeneous subpopulations of subjects maximizing the individual frequency of appearance of clusters from partitions built on their associated M_m matrices.

In the first part of this paper, we will present how to calculate the empirical frequency Q_k of a network R_k based on the comparison of its position in the average dendrogram with respect to the individual dendrograms and then how to use it to identify an unstable network at the population level. Finally, from the individual frequency of a cluster, we will show how to extract, from the initial population, subpopulations that are on average more stable.

2. Presentation of the proposed approaches

Consider M_s ($s = 1, \dots, S$), the S individual correlation matrices of dimension $K*K$.

From the hierarchical ascendant clustering based on the mean matrix M_m defined in the introduction, K nested partitions P_m^j , $j = 1, \dots, K$ can be obtained and summarized by vectors of size K defined as follows. For the partition (also called pattern afterwards) into j clusters, the k^{th} component of P_m^j equal to 1 if the network R_k appears in the new cluster created by switching from a partition into $(j+1)$ clusters to a partition into j clusters. In the following, we will note:

$$P_m = \{P_m^1, \dots, P_m^j, \dots, P_m^K\}$$

with $P_m^1 = (1, \dots, 1)$ et $P_m^K = (0, \dots, 0)$ by convention.

In the same way, for each subject s , the corresponding K nested partitions can be constructed from the M_s matrices:

$$P_s = \{P_s^1, \dots, P_s^j, \dots, P_s^K\} \text{ for } s = 1, \dots, S.$$

For each non-trivial¹ partition from M_m , we will search, among the $(K-2)$ non-trivial partitions of each subject s , the element of P_s closest to P_m^j based on the Sorensen-Dice index defined as follows:

$$C_s^j = 1 - \min_{l=2, \dots, K-1} \frac{2(P_m^j)'P_s^l}{(P_m^j)'P_m^j + (P_s^l)'P_s^l},$$

where the notation v' denotes the transpose of the vector v . A zero index C_s^j (respectively equal to 1) indicates that the vectors P_m^j and P_s^j are equal (respectively, do not share a common network).

In the following, we call “*alternative pattern*” to P_m^j , denoted by \tilde{P}^j hereafter, the pattern(s) of P_s closest to P_m^j in the sense of the index C_s^j (if this pattern is not equal to the average pattern P_m^j).

From the set of the \tilde{P}^j ’s, it is then possible to calculate a Q_k score of participations for each network R_k . This score Q_k represents the empirical frequency (expressed in %) that the network R_k is constitutive of an alternative pattern whatever the average pattern. For an average pattern P_m^j , let us define F^j as the number of single subjects expressing the alternative pattern \tilde{P}^j , and let F_k^j be the number of single subjects expressing the alternative pattern \tilde{P}^j

¹ Partitioning into one cluster (respectively into K clusters) is considered as trivial.

containing the network k . The empirical frequency Q_k of a network R_k is then defined as follows:

$$Q_k = \frac{\sum_{j=1}^{K-2} F_k^j}{\sum_{j=1}^{K-2} F^j}$$

Note. An alternative pattern of P_m^j can never be equal to an average pattern P_m^l of another level than $l \neq j$.

2.1. Method for identifying an unstable network

From the participation score Q_k of each network R_k , it is possible to identify among the K networks the one that will be said to be "unstable", i.e. a network that will not be stable with respect to P_m across the subjects. Typically, a network R_{k^*} that "roams" on the dendrogram associated with P_m , without having a fixed attachment within the S individual dendrograms P_s , leads to an unstable mean tree. The network showing the most marked instability is obtained by :

$$k^* = \arg \max_{k=1, \dots, K} Q_k.$$

By convention, if $Q_1 = \dots = Q_K$, it is considered that there are no unstable networks.

2.2. Method for identifying subpopulations of subjects

Let's first define the individual frequencies of the "average" dendrogram patterns P_m^j denoted F_m^j as the number of single subjects expressing P_m^j .

First, the methodology consists in iteratively selecting the subjects belonging to the pattern $P_m^{j^*}$ such that $j^* = \arg \min_{j=2, \dots, K-1} F_j$. At each iteration, the selected subjects then form a new subpopulation, and the new current population is composed of the unselected subjects. The stopping criterion is to obtain a tree in the current subpopulation such that $\forall j, F_m^j = 1$.

In order to counteract the presence of noise in the data, the cophenetic correlation d (Sokal and Rohlf, 1962) between each of the dendrograms obtained from the mean matrix of each identified subpopulation is then calculated. This allows to group subjects belonging to subpopulations based on cophenetic correlations above a fixed threshold t . The choice of t is left to the user: however it should be noted that the threshold t 1) directly influences the creation of subpopulations, 2) allows the reduction of noise in the tridimensional data, if noise is present. A high value of t (i.e. close to 1) will be recommended if similar populations in the three-dimensional data is suspected, close to 0.5 otherwise. To do this, we set up the following

iterative procedure; we calculate the matrix of cophenetic correlations between the mean dendrograms of the subpopulations obtained at the end of the first step. Thereafter, we threshold this matrix according to t , i.e. correlations lower than t are set to 0. From this matrix, we construct the d -weighted graph G , where each node represents a subpopulation. Thanks to the Louvain method (Blondel et al., 2008) an optimal partition number is obtained by maximizing the modularity of the G graph. Subsequently, the subpopulations are grouped together according to the Louvain partitioning, then a new cophenetic correlation matrix is computed from the mean dendrograms of these new subpopulations and the Louvain partitioning procedure is repeated until G has only one node.

This procedure thus leads to iteratively extracting the most stable subjects from the “average” current $P_{m}^{current}$ dendrogram. It should be noted that by construction, $P_{m}^{current}$ will vary in terms of the arrangement and composition of its scores.

Finally, this procedure is able to identify the existence of a subpopulation of subjects with a pattern that differs constantly within it, or the existence of a subpopulation that does not have a strong structure in terms of dendrogram.

Procedure 1 Identification of subpopulations

Input: F_m^j , individuals, P_m^j

repeat (i times)

$group_i \leftarrow individuals \in P_m^{j*}, j^* = \arg \min_{j=2, \dots, K-1} F_j$

$currentPopulation \leftarrow individuals \notin group_i$

$(F_m^j, P_m^j, Dend_i) \leftarrow individual_frequency_extraction(currentPopulation)$

until $\forall j, F_m^j = 1$

repeat

$matriceD \leftarrow cophenetic(Dend_i)$

$matriceD < t \leftarrow 0$

$modules \leftarrow Louvain(graphFromMatriceD)$

$subPopulation \leftarrow individuals \in modules$

$Dend_i \leftarrow dendrograms(M_m \in subPopulation)$

until $|graphFromMatriceD| == 1$

Output: $subPopulation$

Where “*Individuals_frequency_extraction*” is the implemented algorithm described in Part 2 in order to extract the individual frequencies of the average dendrogram partitions, “*cophenetic*” is the function that computes the matrix of cophenetic correlations between all the

dendrograms two by two of a list of dendrograms, “*Louvain*” is the implemented Louvain algorithm for identifying modules from a weighted graph G (here each node of the graph is a dendrogram composed of s individuals), and “*dendograms*” is the function computing the dendrogram from M_m .

3. Study of numerical behavior

The numerical behaviour of the two proposed methodologies is illustrated on simulated “fMRI-type” data.

- In the first simulation study, we consider a population of S subjects whose correlation matrices M_s , $s = 1, \dots, S$ are “close” (in terms of “mean” dendrogram), except for a network R_{k*} which is randomly permuted for each subject. The objective here is to detect this unstable network which makes the “mean” dendrogram P_m not very representative of the population of S subjects.
- In the second simulation study, the population of S subjects is composed of two subpopulations of homogeneous subjects (in terms of the “average” dendrogram). The objective here is to identify these two subpopulations.

Data simulation. In order to create subjects “close to each other” in the population (or subpopulation), we introduce a correlation matrix M that we will “noise” with a Gaussian random error ε centered with a standard deviation σ as follows: for $1 \leq i < l \leq K$,

$$M_{(i,l)} = \tanh(\operatorname{arctanh}(M_{(i,l)}) + e_{(i,l)}) \text{ et } M_{(l,i)} = M_{(i,l)}$$

where $M_{(i,l)}$ denotes the element (i,j) of the matrix M and $e_{(i,l)}$ is a realization of the noise ε .

Different noise levels σ were considered in the simulation study. Naturally, the higher the noise level, the less homogeneous the population (or subpopulation) generated. To make the simulation study interesting, we consider σ values such that the “mean” dendrogram is similar to the un-noised “mean” dendrogram.

Thereafter, we will work with data similar to those presented in the introduction, i.e. correlation matrices consisting of $K = 28$ resting-state networks R_k .

3.1. Simulation 1: identification of the unstable network

In this first simulation, we will generate, for a noise level $0 \leq \sigma \leq 1$ with a step of 0.1 , K groups of $S = 500$ subjects from one of the individual M matrices presented in the introduction. For each noise level and each network, we have randomly permuted² a network

² i.e. switch the values of the corresponding row/column in the correlation matrix

R_k , i.e: for a given noise level σ , we have $K = 28$ groups of $S=500$ subjects. The objective is to detect, for each noise level and for each permutation, the targeted network R_k (i.e. the permuted network) as the unstable network using the proposed methodology.

Using the methodology proposed for a noise level $\sigma = 0$, we can see in Figure 2 that we manage in 89.3% of the cases to detect the permuted network as the one with the highest Q score. Looking more closely, we can see on the average dendrogram of the group before permutation (Figure 3), that for the permutations of the networks R_k (**RN11**, **RN23** and **RN29**) the network R_k^* detected is each time the one which is directly linked to R_k (**RN22**, **RN14** and **RN7** respectively) instead of R_k itself.

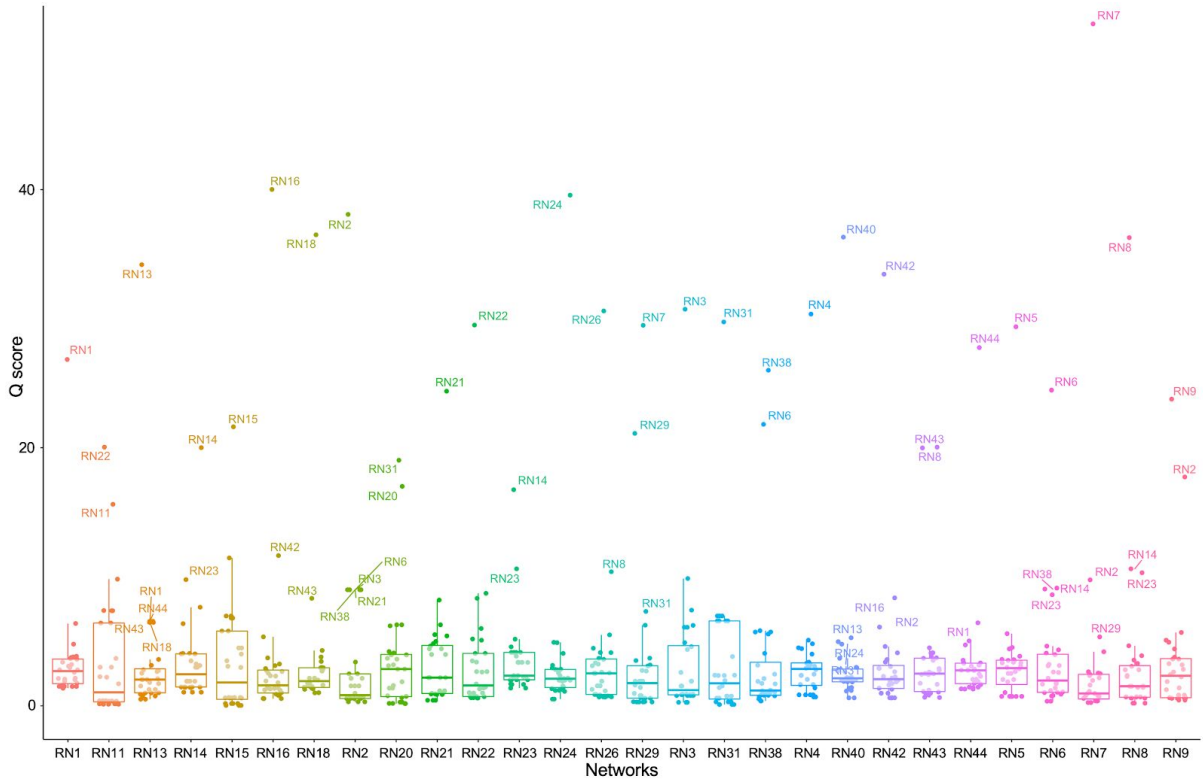


Figure 2: Boxplot of the Q_k score at $\sigma = 0$ for each permutation of K .

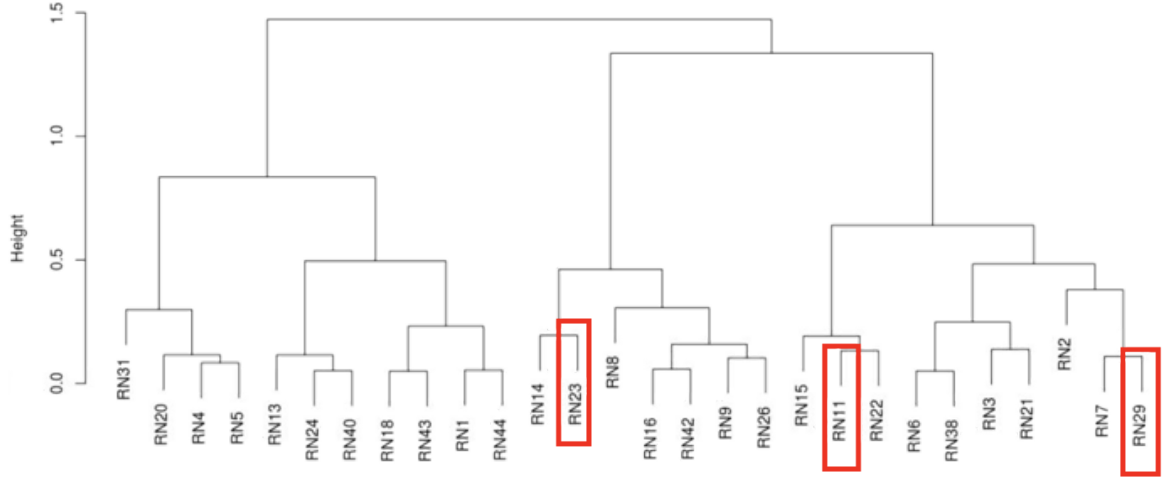


Figure 3: “Average” dendrogram (constructed from M_m) of the population of $S = 500$ subjects before permutation of any network R_k . In red box, permuted R_k networks not detected as k^* at noise level $\sigma = 0$.

Taking the **RN38** network as an example, when we look at the power of the method across all the different noise levels σ (Figure 4), we can see that we are able to detect the correct permuted network (i.e. $R_{k^*} = \mathbf{RN38}$) regardless of the noise level applied to the population of 500 subjects whose network has been permuted. In this example, although **RN38** (in green in Figure 4) is always the network with the highest Q score, the network **RN6** (in yellow in Figure 4) is very close behind. By removing the **RN38** network from the whole population, we can see that the new mean dendrogram is much more stable with only a few alternative “non-dominant” patterns (due to the different noise level); leading to a much higher individual frequency of the mean P_m^k patterns, i.e. to a very low standard deviation of the Q_k score, without a k^* ever actually being detected.

Globally, for the 11 noise levels considered from 0 to 1 (step of 0.1), out of the 28 possible permutations, we detect the correct R_{k^*} (i.e. the permuted network R_k) 95.1% of the time. The 4.9% error corresponds each time to the identification of the network directly linked to the network R_k initially swapped for the simulation.

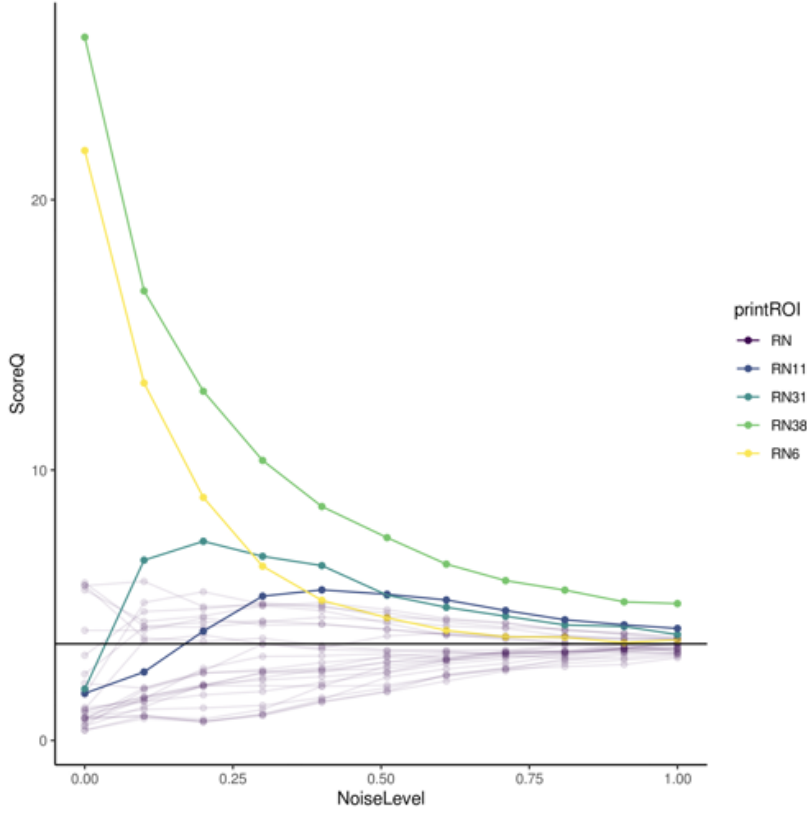


Figure 4: Example of the evolution of the Q_k score of the permuted network $R_k = \mathbf{RN38}$ as a function of the noise level σ in a population of $S = 500$ subjects. The colored curves correspond to the 4 R_k being most often detected as R_{k^*} . In green the target network **RN38**, in yellow the network **RN6** directly linked to **RN38** in the initial dendrogram (see Figure 3).

Our methodology allows us to detect the permuted R_{k^*} network leading to the instability of the mean dendrogram and those regardless of the noise level injected in the data. Note that when σ increases, (there is no more information / common structure in the data), all Q_k scores will converge to $1/k$, i.e. each network participates in many alternative patterns or none of the networks participate in alternative patterns.

3.2. Simulation 2: identification of homogeneous subpopulations.

3.2.1. *Detection of equidistributed population*

In this part, we will consider two populations (G^1_{50} and G^2_{50}) of $S = 500$ subjects. In each population, the subjects are equally divided into two subpopulations A and B of 250 subjects each. For G^1_{50} , the proximity between the mean dendrogram of A and B measured by the cophenetic correlation is 0.18, i.e. subpopulation A is very distant from subpopulation B in terms of the brain organization of their resting-state networks R_k . For G^2_{50} , the cophenetic

correlation between A and B is 0.95, i.e. they are two subpopulations whose brain organization is very close to each other.

Finally, for G^I_{50} and G^2_{50} , we will consider different cases with a noise level σ ranging from 0 to 0.5.

These two case studies, represented by G^I_{50} and G^2_{50} , will allow us to evaluate the subpopulation detection power of our algorithm, in addition to the presence of noise. Concerning the grouping threshold for the part of the method using the Louvain method; $t = 0.8$ for G^I_{50} and $t = 0.99$ for G^2_{50} . Note that the threshold is more restrictive for G^2_{50} since A and B are more similar in this population.

The results for the G^I_{50} study are provided in Table 1. For a null noise level, the algorithm perfectly identifies individuals as belonging to subpopulation A or B. For a noise level $\sigma = 0.12$, the algorithm is able to identify 44% of the individuals belonging to subpopulation A and 36% belonging to population B. For a noise level $\sigma = 0.25$, the algorithm finds more than 50% of the individuals belonging to subpopulation A (28% of individuals identified belonging to this subpopulation), but less than 25% of the individuals belonging to subpopulation B. At the maximum noise level $\sigma = 0.50$, the algorithm finds 11% of individuals from subpopulation A and none from subpopulation B.

The results for the G^2_{50} study are shown in Table 1. In contrast to G^I , the mean dendograms of subpopulations A and B are here similarly closer to each other according to their cophenetic distance (equal to 0.95 for G^2 , 0.18 for G^I). This has a direct impact on the algorithm's ability to identify individuals as belonging to subpopulation A or B. Concerning subpopulation A, the algorithm identifies correctly the individuals for a zero noise level, but the identification drops to 24, 1 and 0% as it increases, which is worse than for G^I . Same results are obtained for the identification of subpopulation B, with results half as good as for G^I .

For a noise level σ multiplied by 2, the proportion of individuals identified as belonging to subpopulation A or B tends to be divided by 2. Moreover, in view of the results, subpopulation B of G^I_{50} seems less stable on average than subpopulation A, the opposite is true for G^2_{50} .

Equitably distributed population (50% A & 50% B)								
	Subpopulation A				Subpopulation B			
	$\sigma = 0$	$\sigma = 0.12$	$\sigma = 0.25$	$\sigma = 0.50$	$\sigma = 0$	$\sigma = 0.12$	$\sigma = 0.25$	$\sigma = 0.50$
Group 1	50	44	28	11	50	36	12	0
Group 2	50	24	1	0	50	17	8	11
Not equitably distributed population (75% A & 25% B)								
	Subpopulation A				Subpopulation B			
	$\sigma = 0$	$\sigma = 0.12$	$\sigma = 0.25$	$\sigma = 0.50$	$\sigma = 0$	$\sigma = 0.12$	$\sigma = 0.25$	$\sigma = 0.50$
Group 1	75	65	64	0	25	11	0	0
Group 2	75	58	33	10	25	0	21	0

Table 1: Evolution of the detection of subpopulations A (in green) and B (in red) according to the evolution of the noise level σ in Group 1 (G^1) and 2 (G^2). Equidistributed population: Group G^1_{50} , cophenetic correlation between A and B of 0.18, 50% of subjects of each subpopulation A and B . Group G^2_{50} , cophenetic correlation between A and B of 0.95, 50% of subjects of each subpopulation A and B . Not equidistributed population: Group G^1_{75} , cophenetic correlation between A and B of 0.18, 75% of subjects of the subpopulation A and 25% of B . Group G^2_{75} , cophenetic correlation between A and B of 0.95, 75% of subjects of the subpopulation A and 25% of B .

3.2.2. *Detection of not equidistributed population*

In this part, we will consider two populations (G^{1bis} and G^{2bis}) of $S = 500$ subjects. In each of the populations, the subjects are equally divided into two subpopulations A and B of 375 subjects for A and 125 for B . For G_1 , the proximity between the mean dendrogram of A and B is the same as in the previous part, as the grouping threshold for the part of the method using the Louvain method.

Finally, for G^{1bis} and G^{2bis} , we will simulate different cases with a noise level σ ranging from 0 to 0.5.

The simulation results are available in table 1. Concerning subpopulation A for G^{1bis} and G^{2bis} , the algorithm identifies more than 85% of its individuals up to a noise level $\sigma = 0.25$. As for the equitably distributed subpopulations, the algorithm manages to identify 100% of the individuals belonging to the different subpopulations when the noise level is zero, and 0% when $\sigma = 0.50$ (exception for G^{2bis} where 10% of the individuals of subpopulation A are correctly identified).

Again, we can note that, the more noise increases, either one of the two groups A or B disappears, or the more the number of subjects belonging neither to A nor to B increases, up to a rate of 100%.

We can note, from Figure 6, that the subjects detected as belonging to group A or B are initially subjects belonging to these groups (very low noise error rate). Secondly it is interesting to note that the category of subjects neither belonging to group A or B , is composed of similar proportions to the one we initially injected during the creation of the simulation.

4. A real case study

An example of the application of the method can be read in Doucet et al. (2020).

There is currently no brain atlas of the intrinsic organization of the brain constructed from populations whose individuals are over 40 years of age. However, the brain, and thus the

brain networks that compose it, undergo continuous reconfiguration throughout adult life (Damoiseaux, 2017; Yaple et al., 2019). The absence of brain atlases from older populations therefore directly influences the results related to the different properties of intrinsic networks. In this context, the objective of the study was to construct a reliable brain atlas derived only from healthy older participants.

Doucet & al. (2020) analyzed fMRI data from 184 individuals aged 55-80 years from the SALD cohort (*Southwest University Lifespan Dataset*, Wei et al., 2018). Using a multi-step independent component analysis approach, they identified 24 RNs (Figure 5 - A.).

In this framework, our method was used to verify 1) the stability of the identified intrinsic networks (RNs) and 2) the presence of subpopulations in the data (the cophenetic threshold was fixed at 0.85).

We found that no RNs in the SALD sample of individuals aged 55 or older were unstable (Figure 5 - B.).

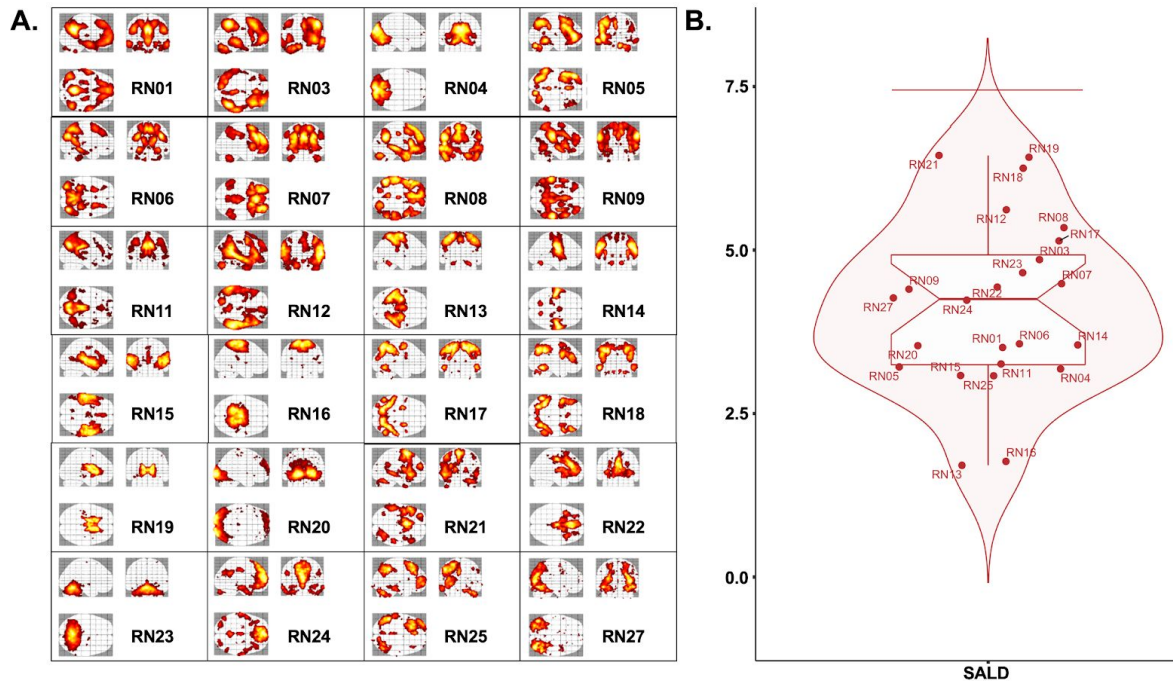


Figure 5: Presentation of the RNs of the SALD cohort and their stability. A. Spatial map of the components obtained from the multi-step independent component analysis on the intrinsic connectivity data of the SALD cohort. B. Tukey box of the stability Q_k score for each network in the SALD cohort. The horizontal red line represents the limit at which a RN is considered unstable (extremum).

In addition, two subpopulations were identified in the SALD cohort (Figure 6). The first one (*Subpopulation 1* in Figure 6) is composed of 85 individuals and has a mean age of

62.5 years old. The second one (*Subpopulation 2* in Figure 6) of 94 individuals of 64.5 years old in average. Two-tailed Student's t-test revealed no difference between the 2 subpopulations in terms of demographics variables (Edinburgh test : $p = 0.8$, sexe : $p = 0.15$, Pearson's chi-squared test), neither in anatomical variables (Total Intracranial Volume : $p = 0.81$) or in quality control variable (all $p > 0.2$). One-tailed t-test revealed a significant inferior average age in the first Subpopulation than in second one ($p = 0.032$).

A comparison of the average dendrograms of the two subpopulations highlights the existence of 2 partitions in each subpopulation. The first one includes RNs related to the extrinsic system (blue rectangles in Figure 6): *i.e.* a system driven by external inputs and activated during sensory stimulations, including the attentional and the sensory-motor network. The second partition corresponds to the intrinsic system (Red rectangle in Figure 6) that is used in inner-oriented mental activity.

This organization of resting-state brain processes corresponds well to the organization highlighted in Doucet & al. (2011). The calculation of the cophenetic distance between the two means dendrograms of the 2 subpopulations was 0.76, revealing two slightly different organizations. The main difference between the 2 subpopulations (Figure 6) comes from the networks RN18 and RN17 which in the case of subpopulation 1 belongs to the extrinsic system, whereas these RNs belong to the intrinsic system in the second. The RN18 corresponds to one of the fronto-temporo-parietal network, involved during the executive processes of selecting and monitoring our behaviours. The RN17 corresponds to the spatial attention network. These two RNs are grouped together very early in the 2 dendrograms, thus we can tentatively identify this couple as being a marker of the resting state activity either turned towards the outside, or towards oneself.

This organizational difference, possibly related to age (compared to young subjects, Doucet & al., 2011), deserves to be addressed more in-depth study with complementary neuroscientific approach, such as the resting state questionnaire for evaluation of inner experience during the conscious resting state (Delamillieure & al., 2010).

.

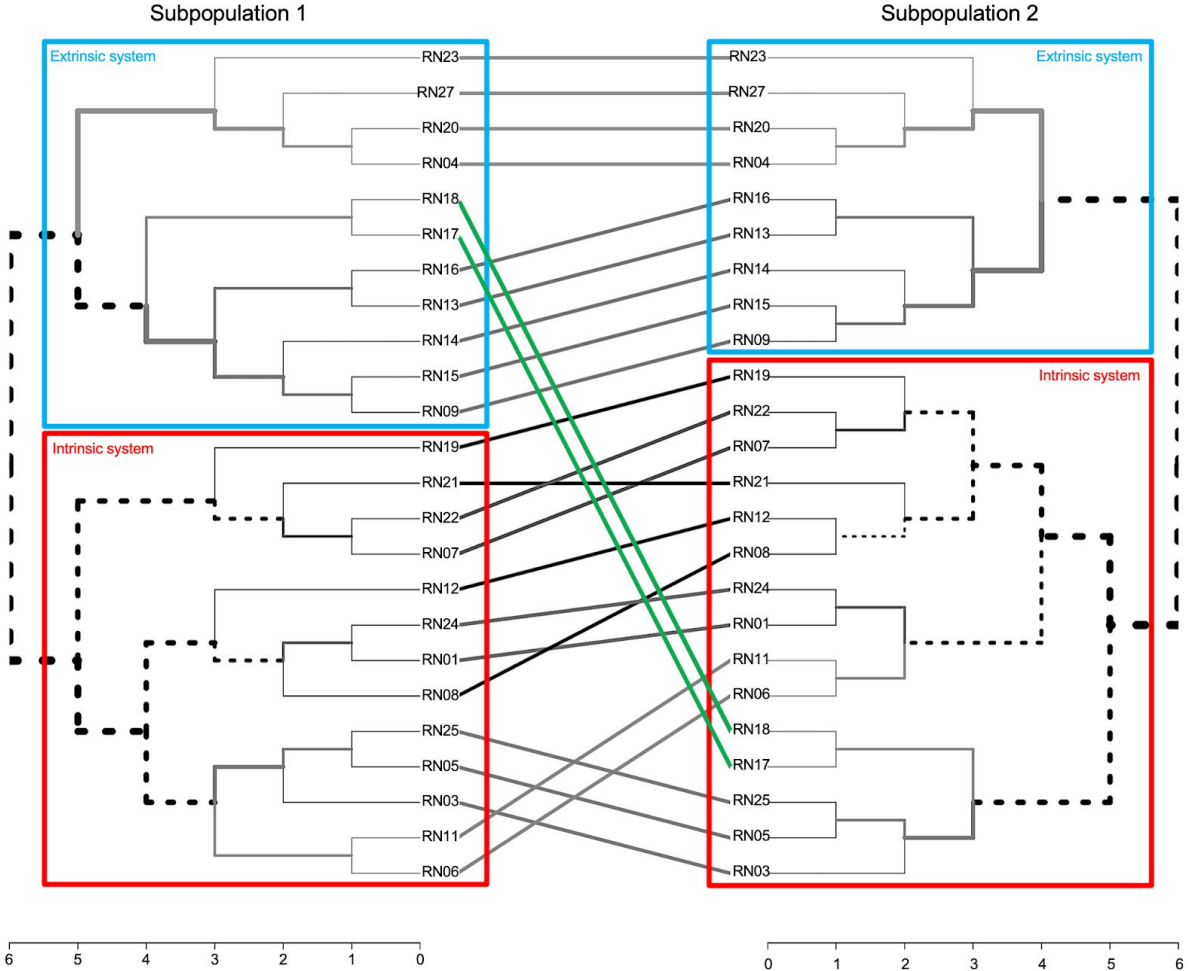


Figure 6: Tanglegram between subpopulations in the SALD cohort. The red rectangle represents the intrinsic system; in blue the extrinsic system. The green lines correspond to the two RNs whose positioning in the mean dendrogram differs from one subpopulation to another.

5. Concluding remarks

We have here introduced two different techniques allowing 1) to analyse the stability of the constituent features of an average dendrogram produced from three-dimensional data: the Q_k score, and 2) to extract homogeneous subpopulations in terms of individual dendograms from three-dimensional data.

The first one is based on the new reliability Q_k score introduced in Section 2. This core represents the relative position of the network k across the individual dendograms, relative to the average dendrogram. The simulation study provided good numerical performance of the proposed methodology.

Furthermore, the second proposed approach is able to identify the existence of a subpopulation of subjects with a pattern of features that differs constantly within it, or the existence of a subpopulation that does not have a strong structure in terms of dendrogram.

Concerning the capacities of the algorithm to identify subpopulations, the similarity between subpopulations, the proportion of each subpopulation directly influences the performance of the algorithm. A subpopulation which is small in number of individuals and whose mean dendrogram is not singular: i.e. whose cophenetic distance is high in relation to the mean dendrogram of the other subpopulations, will be difficult to identify. In contrast, a large subpopulation with a singular dendrogram will be easy to identify. The modulation of the threshold value t comes into play here, a t value close to 1 allowing a better distinction between two similar dendograms according to the cophenetic distance.

These two new methods will soon be available via a library called **SIMS** (*Similarity of Individual MatriceS*) on GitHub, then on CRAN, it can also be directly requested from the corresponding author.

References

Blondel, V. D., Guillaume, J.-L., Lambiotte, R., & Lefebvre, E. (2008). Fast unfolding of communities in large networks. *Stat. Mech.* (2008) P10008, 0803.0476v2.

Charrad, M., Ghazzali, N., Boiteau, V., & Niknafs, A. (2014). NbClust: An R Package for determining the relevant number of clusters in a data set. *Journal of Statistical Software*, 61(6), 1-36.

Damoiseaux, J. S. (2017). Effects of aging on functional and structural brain connectivity. *Neuroimage*, 160, 32-40.

Delamillieure, P., Doucet, G., Mazoyer, B., Turbelin, M. R., Delcroix, N., Mellet, E., ... & Joliot, M. (2010). The resting state questionnaire: An introspective questionnaire for evaluation of inner experience during the conscious resting state. *Brain research bulletin*, 81(6), 565-573.

Doucet, G., Naveau, M., Petit, L., Delcroix, N., Zago, L., Crivello, F., . . . Joliot, M. (2011). Brain activity at rest: a multiscale hierarchical functional organization. *J Neurophysiol*, 105(6), 2753-2763.

Doucet, G. E., Labache, L., Thompson, P. M., Joliot, M., & Frangou, S. (2020). Atlas55+: brain functional atlas of resting-state networks for late adulthood. *BioRxiv* 2020.07.13.200824; doi: <https://doi.org/10.1101/2020.07.13.200824>.

Efron, B. (1985). Bootstrap confidence intervals for a class of parametric problems. *Biometrika*, 72(1), 45-58.

Logothetis, N. K., Pauls, J., Augath, M., Trinath, T., & Oeltermann, A. (2001). Neurophysiological investigation of the basis of the fMRI signal. *Nature*, 412(6843), 150-157.

Mazoyer, B., Mellet, E., Perchey, G., Zago, L., Crivello, F., Jobard, G., . . . Tzourio-Mazoyer, N. (2016). BIL&GIN: A neuroimaging, cognitive, behavioral, and genetic database for the study of human brain lateralization. *Neuroimage*, 124(Pt B), 1225-1231.

Schummers, J., Yu, H., & Sur, M. (2008). Tuned responses of astrocytes and their influence on hemodynamic signals in the visual cortex. *Science*, 320(5883), 1638-1643.

Sokal, R. R., & Rohlf, F. J. (1962). The comparison of dendograms by objective methods. *Taxon*, 11(2), 33-40.

Suzuki, R., & Shimodaira, H. (2004). An application of multiscale bootstrap resampling to hierarchical clustering of microarray data: How accurate are these clusters. *The Fifteenth International Conference on Genome Informatics*, 34.

Suzuki, R., & Shimodaira, H. (2006). Pvclust: an R package for assessing the uncertainty in hierarchical clustering. *Bioinformatics*, 22(12), 1540-1542.

Wei, D., Zhuang, K., Ai, L., Chen, Q., Yang, W., Liu, W., ... & Qiu, J. (2018). Structural and functional brain scans from the cross-sectional Southwest University adult lifespan dataset. *Scientific data*, 5, 180134.

Yaple, Z.A., Stevens, W.D., Arsalidou, M., 2019. Meta-analyses of the n-back working memory task: fMRI evidence of age-related changes in prefrontal cortex involvement across the adult lifespan. *Neuroimage* 196, 16-31.